Using artificial intelligence methods for shear travel time prediction: A case study of Facha member, Sirte basin, Libya

Bahia M. Ben Ghawar[*], Moncef Zairi, Samir Bouaziz

Ecole Nationale d'Ingénieurs de Sfax, University of Sfax, Tunisia
[*]*Corresponding author: gloriamuftah@yahoo.com*

Abstract

Shear wave travel time logs are major acoustic logs used for direct estimation of the mechanical properties of rocks. They are also important for prediction of critical drawdown pressure of the reservoir. However, core samples are sometimes not available for direct laboratory measurements, and the time-consuming dipole shear imager tool is generally not used. Hence, there is a need for simple indirect techniques that can be used reliably. In this study, cross-plots between the available measured shear travel time and compressional travel time from three oil wells were used, and three artificial intelligence tools (fuzzy logic, multiple linear regression and neural networks) were applied to predict the shear travel time of Facha member (Gir Formation, Lower Eocene) in Sirte Basin, Libya. The predicted times were compared to those obtained by the equation of Brocher. The basic wireline data (gamma ray, neutron porosity, bulk density and compression travel time) of five oil wells were used. Based on principle component analysis, two wireline data sets were chosen to build intelligent models for the prediction of shear travel time. Limestone, dolomite, dolomitic limestone and anhydrite are the main lithofacies in the Facha member, with an average thickness of about 66 m. The simple equation gave 87% goodness of fit, which is considered comparable to the measured shear travel time logs. The Brocher equation yielded adequate results, of which the most accurate was for the Facha member in the eastern part of the Sirte basin. On the other hand, the three intelligent tools' predictions of shear travel time conformed with the measured log, except in the eastern area of the basin.

Keywords: Carbonate Rock; intelligent tools; Libya; shear travel time; sirte basin.

1. Introduction

The dipole shear imaging logging tool measures both compressional ($\Delta Tc = 1/Vp$) and shear ($\Delta Ts = 1/Vs$) travel time waves to estimate the mechanical properties of rocks (Liu, 2017; Bateman, 2012). However, when ΔTs is not measured (*i.e.*, in old wells) or cannot be measured (*i.e.*, in soft formations or poor cement jobs), synthetic shear travel times are computed using other petrophysical data. Therefore, many empirical relations for estimating shear velocity (Vs) from compressional velocity (Vp) have been published, but most of them are established for clastic rocks, carbonate rocks and coal. For example, the Greenberg & Castagna ,(1992) relation is easily applied and commonly used, but it is unsuitable for anhydrite rock, such as at the site described in the current study.

Therefore, methods based on rock physics are being developed. Miraj *et al*., (2021) used seismic line and wireline log data to define the structural features and hydrocarbon potential of rock. Also, Tao *et al.,* 2020 applied high-density resistivity and shallow seismic reflection methods in a mine in Shandong, China to define the cause of subsidence. Different techniques were applied on a reduced-to-magnetic equator (RTE) anomaly map to define geologic features and their geometry, which included solid minerals emplacement in the Igbeti-Moro area of southwestern Nigeria (Olasunkanmi *et al.,* 2020). Singh & Kanli, (2015) applied a back-propagation artificial Neural Network (ANN) based on neutron porosity, density, true resistivity, compressional wave velocity and gamma ray logs as input data. They demonstrated good correlation between shear velocity estimated by the ANN and an empirical equation. In another context, Amiri *et al.,* (2018) used NN to predict precipitation in two provinces in Iran.

Furthermore, Khamehchi *et al.,* (2014) estimated critical total drawdown as an index of sand production onset from the data of 23 problematic wells in the North Adriatic Sea. The authors started with simple linear regression, MLR and genetic algorithm evolved MLR to estimate critical total drawdown. They then developed two ANN with back propagation and particle swarm optimization algorithms. The study demonstrated the performance and accuracy of the artificial neural networks in predicting sanding onset. Also, well logging data at the BD Madura gas field were used to calculate drilling geological and mechanical parameters. The results were used to estimate drilling risk probability distributions as a function of pore pressure and equivalent circulation fluid density (ECD) as uncertainty analysis (Guan *et al.,* 2018).

Carbonate rocks are common reservoir rocks in the western part of Sirte Basin (Zallah Trough), and petrophysics studies generally focus on reservoir evaluation. However, most exploration wells do not have ΔTs logs and lack some of the basic wireline data such as neutron porosity and litho-density logs. Therefore, prediction of ΔTs of the Facha reservoir requires the development of a geomechanical model in order to minimize drilling problems and instability in newly developed wells. Loss of circulation was recognized in two wells located in Dahab and Ghani oil fields in the lower part of the Facha member, and was attributed to a change of rock type from porous dolomite to limestone. Different intelligent tools can be used to predict ΔTs in carbonate lithofacies, and these predictions can be compared with both simple cross-plot regression and the results of the Brocher, (2005) equation. Here, the intelligent tools, the Brocher equation and the simple cross-plots of measured travel times were applied to data from five oil wells in the Ghani oil field, El Nagah field, Mabrouk area, and Sarir trough in Libya to find a suitable prediction tool for generating synthetic ΔTs logs.

2. Geological background

The Sirte Basin is one of the main hydrocarbon provinces of Libya with clastic (pre-Tertiary) and carbonate (Tertiary) reservoirs. Platforms and troughs are the main structural features of the basin in the northwest to southeast trend (figure. 1).

The structural setting of this basin was postulated based on continental rifting (extensional) related to evidence of Cretaceous–Tertiary events (Hallett & El Ghoul, 1996; Gras, 1996; Guiraud, 1998; Tawadros, 2001; Ahlbrandt, 2001). Abdunaser & McCaffrey, (2014) interpreted the structural configuration of Sirte basin as related to the African plate motion. Accordingly, Sirte Arm, Tibesti Arm and Sarir Arm are the three main rifting arms

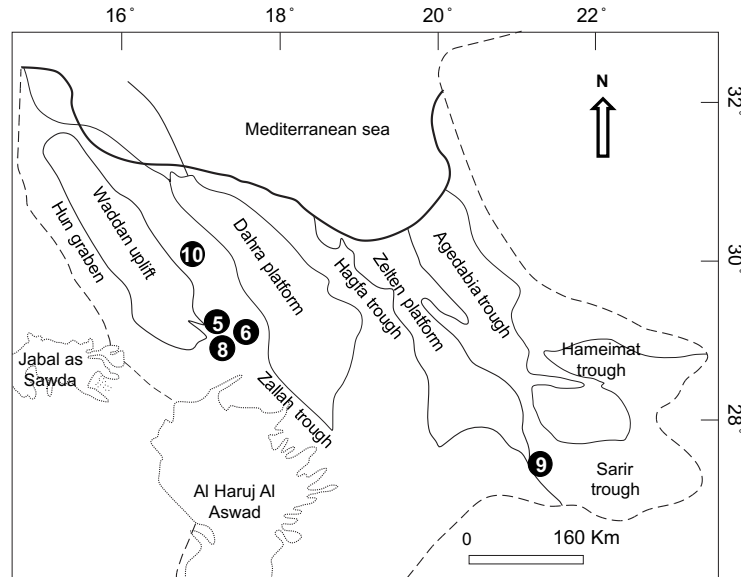formed in early Cretaceous and early Tertiary (Harding, 1984; Gras & Thusu, 1998; Ambrose, 2000).

Fig. 1. Study area and wells location

Three troughs (Dur al Abd, Zallah and Abu Tumayam) have a northwest-southeast direction in the western part of the Sirte Basin. These troughs are asymmetric from the north to the south trend, with the northeast tilting towards Ajdabiya (Hallett & Lowes, 2017). The formations of Gir, Beda, Dahra, Zelten and Farrud are the major reservoir rocks in the western Sirte Basin. The Gir Formation of Lower Eocene (Mijalkovice, 1977; Banerjee, 1980) has a thickness of about 610 meters (Barr & Weeger, 1972). Also, Facha member, Hon Evaporite member and Mesdar Limestone member are parts of the Gir Formation with different lithofacies (figure 2).

Age		Stratigraphic unit Fm. Mbr.		Lithology	Description
Tertiary	Lower Eocene	Gir	Mesder		Limestone and anhydrite interbedding
			Hon Evaporite		Salt and dolomite interbedding within thick anhydrite beds
			Facha		Dolomite with anhydrite and shaly limestone

Fig. 2. Generalized stratigraphic section of the Gir Formation.

The variety of lithofacies is due to three depositional environments: deep marine outer shelf, shallow marine inner shelf and restricted shelf. The restricted condition, which includes lagoon, tidal flats, sabkhas, bays, ponds and subbasins (Abugares, 1996), is prevalent in the Zallah trough. Therefore, the rock types of the Facha member are limestone, dolomite, dolomitic limestone and anhydrite, with the dolomite being predominant. Lashhab & West, (1996) and Elag , (1996) demonstrated an early and late diagenetic dolomitization phases and classified the dolomite into microsparitic crystalline, fine-to-medium crystalline, and coarse-grained dolomite.

3. Methodology for predicting ΔTs

The major basic wireline data recorded in wells 5, 6, 8, 9 and 10 are GR, ΔTc, ΔTs, Øn, ρb, photoelectrical factor (PEF), caliper (CAL), and electrical resistivity (induction, laterolog or array). Figure 3 illustrates the workflow for the processing track of these data to define a suitable prediction model for the shear travel time of the Facha member.
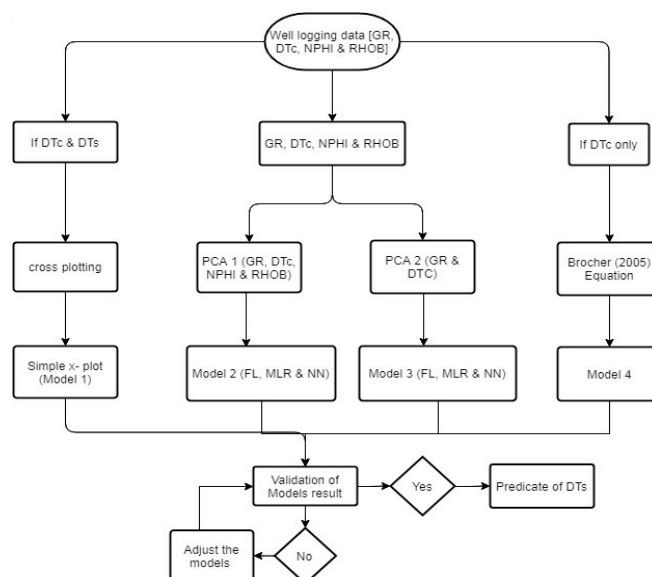

Fig. 3. Workflow of a process for shear travel time prediction

Data from wells 5, 6 and 8 were used to construct simple or direct cross-plots between measured interval travel times, and models were built by using intelligent tools. Wells 10 and 9 were used for models validation. The Øn, ρb and PEF logs were used to discriminate the Facha lithofacies by cross-plots of ρb–Øn and ρb–PEF. Data of the measured shear and compressional interval travel time (DSI logs) of wells 5, 6 and 8 were used to construct simple cross-plots of the Facha member.

Interactive Petrophysics (version 4.2) was used for principal component analysis (PCA), FL, MLR and NN tools to construct the best model for ΔTs prediction. Different sets of basic measured wireline data (GR, ΔTc, Øn and ρb) were used as input. Equation 1 (Brocher, 2005), which is dependent on log (Vp = 1/ΔTc), was used for different lithologies with primary velocities (Vp) between 1.5 km/sec and 8.5 km/s (Maleki *et al.*, 2014).

$$V_S = 0.7858 - 1.2344\,V_P + 0.7949\,V_P^2 - 0.1238\,V_P^3 + 0.006\,V_P^4 \tag{1}$$

where Vp = sonic velocity (compressional velocity = 1/ΔTc, km/s), Vs = sonic velocity (shear velocity = 1/ ΔTs, km/s), ΔTs = shear travel time (μsec/ft), and ΔTc = compressional travel time (μsec/ft).

The PCA is used to reduce multidimensional data sets to lower dimensions for analysis. The PCA curves can be used for multi-well tops correlation and regression analysis. The FL curve prediction module uses FL as described by Cuddy, (1997), which allows the prediction of a result curve from a number of input curves. In fuzzy estimation, the number of bins was set to 10 for training divided data. Thus, the two statistics parameters μ and σ are calculated of

each data bin and used to compute the FL average probability. Whereas the MLR allows the prediction of a result curve from a number of input curves, the least squares regression routine is intended to find the best fit to the input data.

The same well-logging input data of the PCA, FL and MLR were used in the NN tool with one input layer, one hidden layer and one output layer. The trial zones were selected in front of input data curves at different depths of the Facha member. Training passes, epoch per pass and cross-validation percentage are three training settings of the NN technique. The training passes specify how many times the NN will be trained each time, and in this case, it was 3. The epoch per pass shows how many times the training data will be taken, and in this case, it was 100. The cross-validation percentage of the input data defines how much of the training data cross-check to process, and this was 5%. Epochs trained, the epoch of best cost and raw sensitivity are four outputs of the training settings. Therefore, after training the tool many times, it was used to build the NN model.

4. Results and discussion

Figure 4 shows a plot of bulk density (ρb) versus neutron porosity ($\varnothing$n) in four wells, illustrating the average matrix density (ρma) lines of different lithology; Sandstone = 2.65 g/cm^3, Limestone = 2.71 g/cm^3, Dolomite = 2.87 g/cm^3 and Anhydrite = 2.98 g/cm^3. Most of the plotting points fall between the average matrix density lines of limestone rock (2.71 g/cm^3) and anhydrite rock (2.98 g/cm^3). The shifting of the plotted points of wells 5, 6 and 8 from the dolomite line towards the anhydrite line is attributed to the existence of the anhydrite as a cement material, while the plotting points of well 9 fall on the average matrix density of the dolomite line with high values of neutron porosity ($\varnothing$n). The cluster points in the lower part of the plot close to zero neutron porosity and less than 2.8 g/cm^3 of bulk density demonstrate anhydrite lithofacies. Also, anhydrite strips are clearly present within the Facha member at different depths: 3990, 4215 and 4240 ft in well 8 (figure 6). It worth mentioning that well 10 was excluded because no neutron and litho-density logs are available. Therefore, dolomite is the most common rock type in the Facha member, along with limestone, dolomitic limestone and anhydrite.
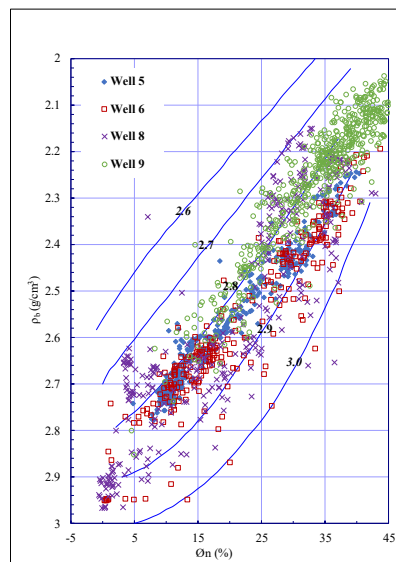

Fig. 4. Cross-plot of bulk density (ρ_b) versus neutron porosity ($\varnothing$n)

The PCA on models run with the first input data set (GR, ΔTc, Øn and ρb) of wells 5, 6 and 8 has a variability of 64.7%, 23.2%, 7.9% and 4.2%, respectively. PCA of the second input set has a variability of 58.6% and 41.3 % for GR and ΔTc, respectively. These two sets of basic well logging data were used to build an intelligent model of ΔTs. The second set of logs enabled the prediction of synthetic ΔTs for wells that had no basic wireline logs, such as well 10, which has neither a Øn nor a ρb log. Wells 9 and 10 were used to validate different ΔTs models. Figure 5 shows a simple plot between measured ΔTs and ΔTc for wells 5, 6 and 8 using 787 data points. A simple regression equation was generated (Equation 2, $R^2 = 0.87$). The model built on MLR used 787 data points from the first and second input data sets from the same wells, and Equations 3 and 4 were extracted with a regression coefficient $R^2 = 0.91$ and 0.89, respectively.

$$\Delta Ts = 3.32 + (1.6 * \Delta Tc) \tag{2}$$
$$\Delta Ts = 122.7 - (0.3 * GR) + (1.3 * \Delta Tc) - (26.7 * Øn) - (33.6 * \rho b) \tag{3}$$
$$\Delta Ts = 14.9 - (0.3 * GR) + (1.5 * \Delta Tc) \tag{4}$$
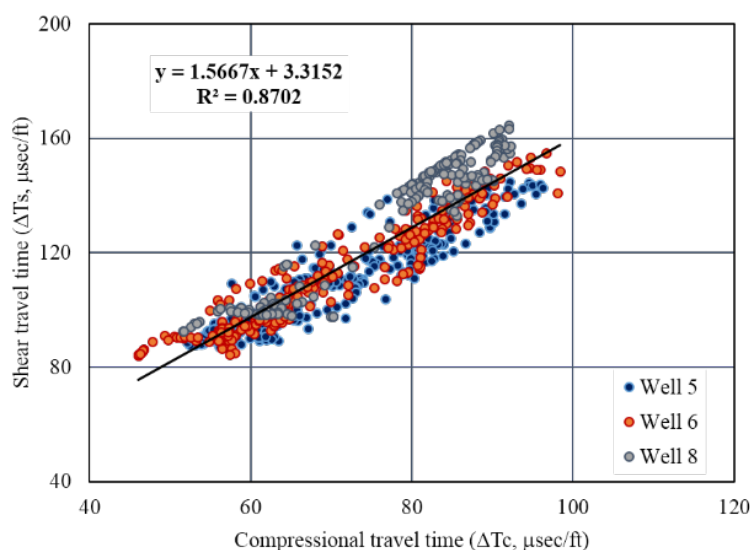

Fig. 5. Plot of log data of measured ΔTs and ΔTc

One stage of training was performed on the NN tool, with the epoch of best cost equal to 65 as the second and third training passes did not improve the first pass. Also, the minimum error of the best cost was equal to 1.4E-314, where a lower value is better.

MLR, NN, simple plot and the Brocher (2005) equation (Equation 1) yielded ΔTs values that generally agreed with the measured values. In wells 5 and 6, ΔTs values derived from the simple cross-plot equation were higher than the measured values in porous dolomite lithofacies. On the other hand, in wells 8, 9 and 10 it was less than the measured log in dolomitic limestone and anhydrite lithofacies. In less porous dolomite lithofacies, ΔTs calculated from simple plots was similar to the measured values (figures 6 and 7). Well 9 is located at the Sarir Trough (southern shelf), and the depositional environment is the shallow carbonate-inner shelf in the Eocene time (Hallett & Lowes, 2017). However, in this well, the simple plot and intelligent

models yielded lower estimations of ΔTs, whereas the Brocher (2005) equation yielded the most accurate estimate (figure 8).

Figure 9 compares the ΔTs of well 10 showing clear agreement between the predicted and measured values, except below the depth of 3430 feet due to the increase of GR. The NN tool gave the best prediction of ΔTs in this well throughout the Facha member.
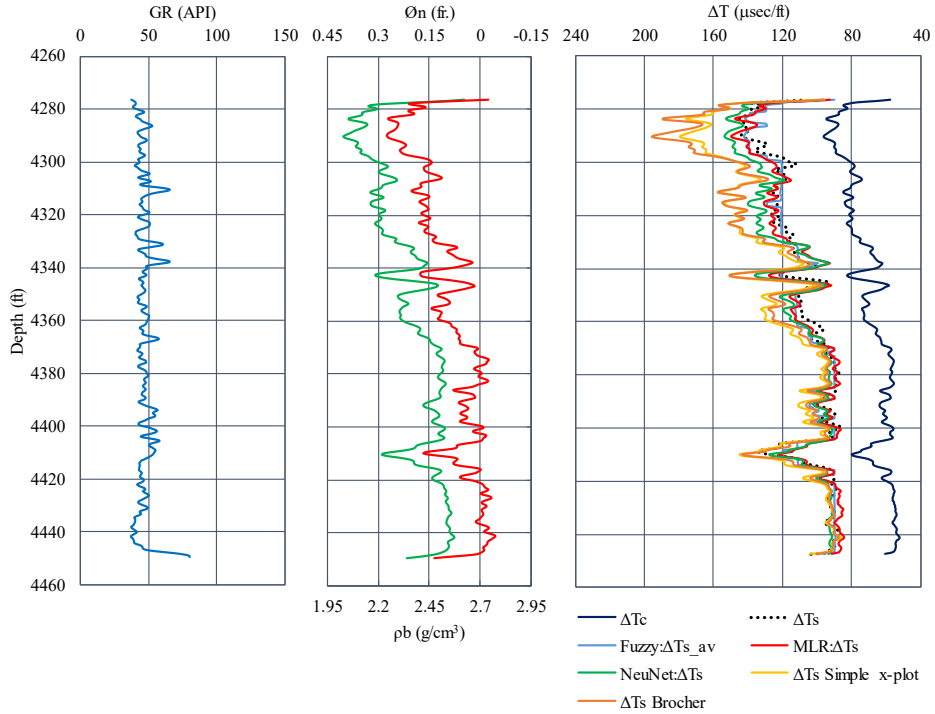

Fig. 6. Measured and predicted ΔTs and basic wireline data of well 5
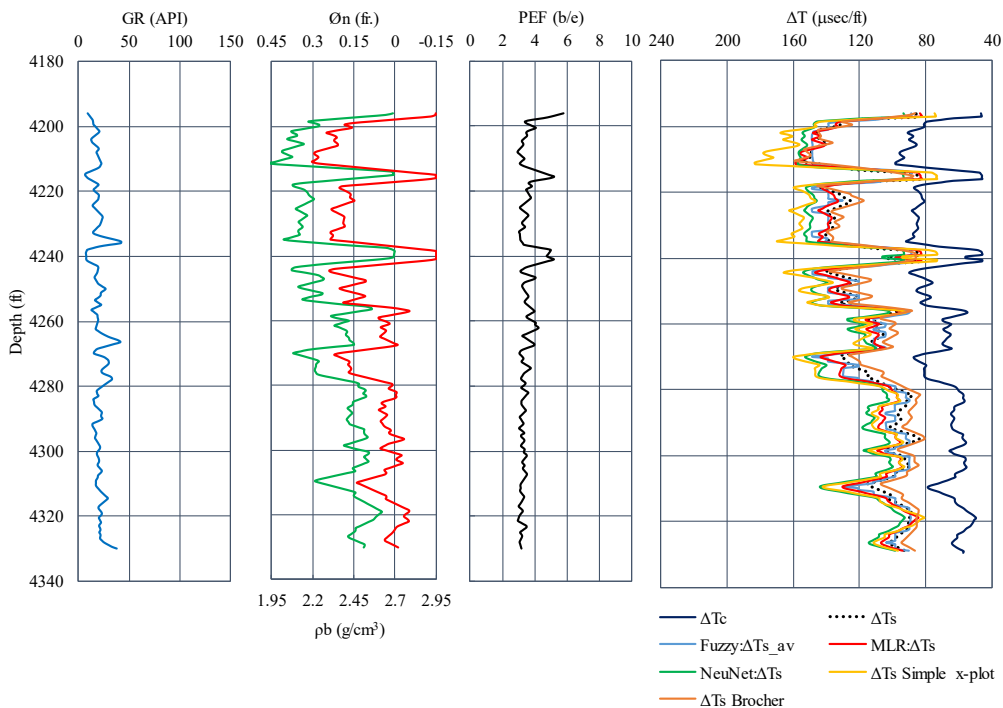

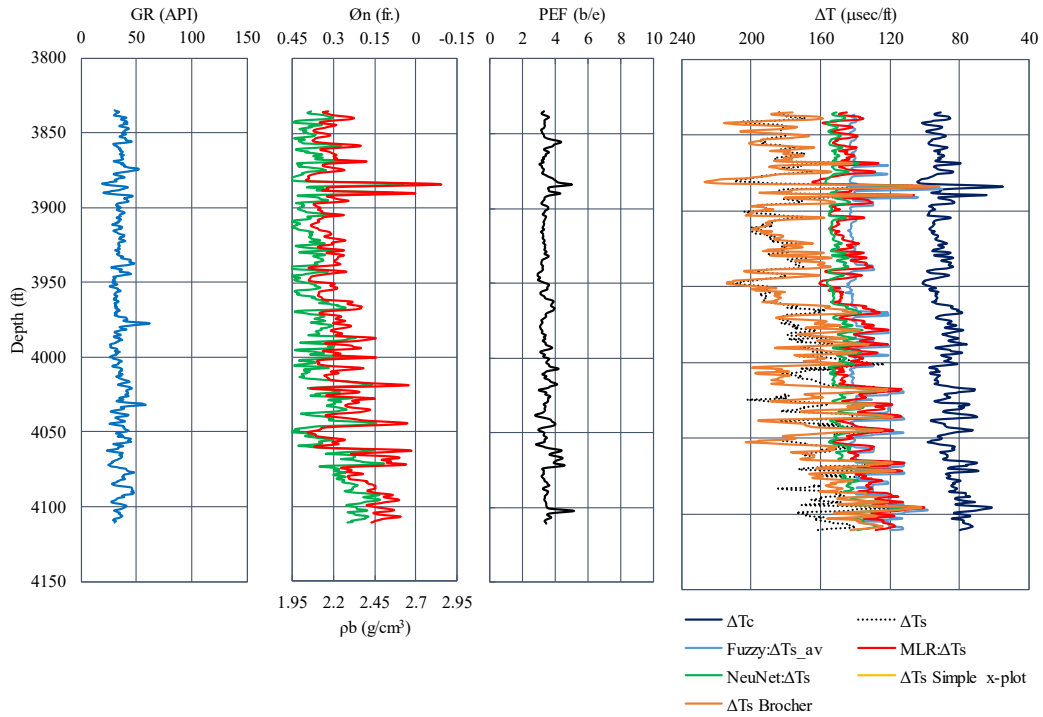**Fig. 7.** Measured and predicted ΔTs and basic wireline data of well 6.

Fig. 8. Measured and predicted ΔTs from basic wireline data of well 9
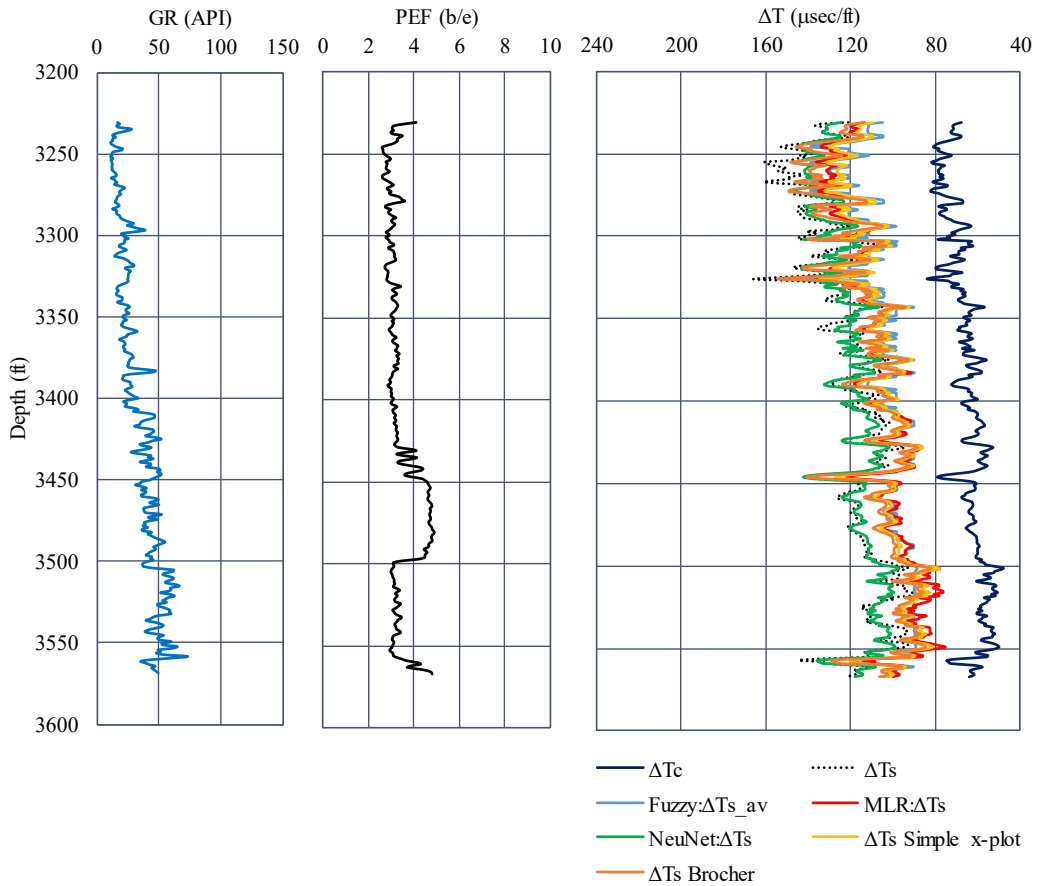

Fig. 9. Measured and predicted ΔTs of well 10, GR and PEF

The statistical analysis tools, IHS Kingdom and IBM SPSS Statistics 20, were applied by Ehsan *et al.,* (2018) to well logs and seismic data to classify reservoir and source rocks depth at Sindh province in the Southern Lower Indus Basin of Pakistan. Hence, the Table 1 summarizes the statistical of error measurements and performance of the models. It includes the average difference between measured and predicted values of ΔTs ($\Delta TsM - \Delta TsP$), standard error (SE), and goodness of fit (R^2). The differences between the measured and predicted values of ΔTs for the first and second input data sets were 5-15 µsec/ft and 4-17 µsec/ft, respectively. The SE of the predicted shear travel time, calculated by using Equation 5, reached up to 19 µsec/ft.

$$SE = \sqrt{\frac{(\Delta TsM - \Delta TsP)^2}{n-2}} \qquad (5)$$

ΔTsM: measured shear travel time (µsec/ft); ΔTsP: shear travel time (µsec/ft) predicted by the different techniques; n = number of data points; SE: standard error.

The Correlation between ΔTsM and ΔTsP for the first input data set for wells 6 and 9 are shown in figure 10. The assessment of the intelligent tools in predicting shear travel time in the Zallah and Sarir Troughs were with the R^2 equal to 0.9 and 0.6, respectively. On the other hand, cross-plots and the Brocher equation were more suitable for the Facha member at different locations in the Sirte Basin, with 90% goodness of fit. The lower R^2 in well 9 could be attributed to dolomitic limestone lithofacies and higher shale content. Similar results have been reported by Akhundi *et al.,* 2014, who applied artificial NN, the Castagna empirical equation and MLR to estimate ΔTs. They found that ΔTs prediction by the ANN was acceptable in relation to the measured values. Also, the MLR yielded predictions with 92% fit, but it cannot be used for generalization across different lithologies. However, the Castagna empirical equation had a correlation coefficient (R^2) of 0.72 and was considered acceptable for use in wells with incomplete well logging data.
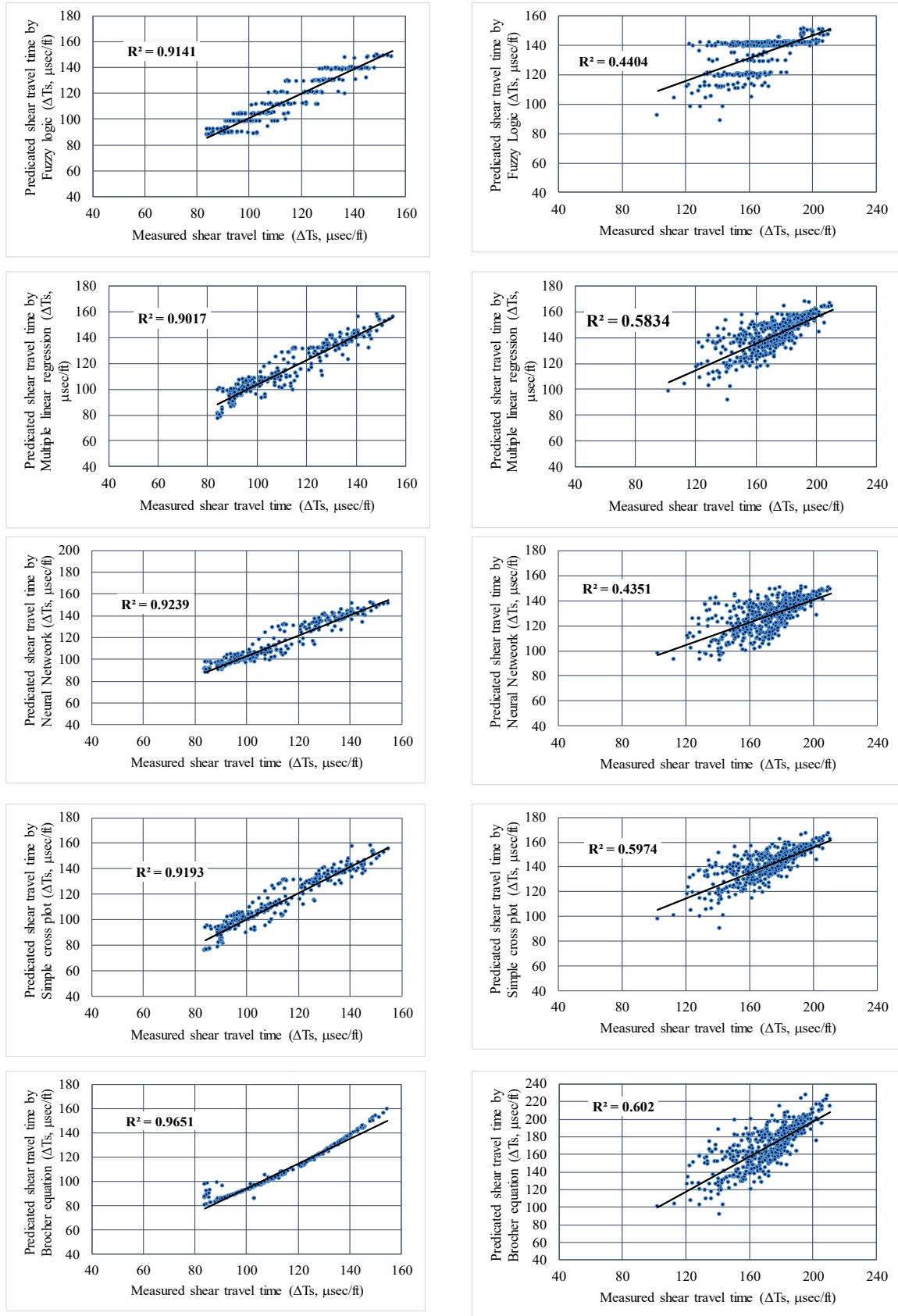
Well 6 | Well 9

Fig. 10. Correlation between measured and predictions ΔTs by different models in wells 6 and 9 by using the first set of data

5. Conclusions

In general, prediction of ΔTs on the basis of GR, ΔTc, Øn, and ρb is important in old wells or wells with borehole problems, such as collapse or caving. Predicted ΔTs is useful for understanding the mechanical behavior of rocks and helpful in dealing with well instability. However, though this approach is applicable to clastic and carbonate rocks, it is not applicable to situations where limestone, dolomite, dolomitic limestone and anhydrite are present, and the use of any empirical equation could be ruled out.

Table 1. Goodness of fit, average difference and standard error of the input data set

Well	Model	1st PCA input data			2nd PCA input data		
		R^2	Difference	SE	R^2	Difference	SE
5	Fuzzy logic	0.83	7.1	10.66	0.89	4.1	5.6
	Multiple linear regression	0.86	4.6	6.25	0.88	4.9	6.3
	Neural Network	0.85	5.4	7.58	0.86	6.8	8.7
	Simple cross plot	0.89	14.1	17.70	-	-	-
	Brocher (2005) equation	0.88	13.4	18.40	-	-	-
6	Fuzzy logic	0.91	4.7	8.06	0.93	4.7	6.2
	Multiple linear regression	0.90	5.8	9.00	0.93	5.2	6.6
	Neural Network	0.92	4.9	8.20	0.92	12.2	13.8
	Simple cross plot	0.91	4.9	8.30	-	-	-
	Brocher (2005) equation	0.96	6.5	8.56	-	-	-
8	Fuzzy logic	0.92	6.9	9.05	0.93	7.7	8.9
	Multiple linear regression	0.89	6.9	8.99	0.94	7.5	8.7
	Neural Network	0.93	8.6	12.2	0.95	4.8	6.7
	Simple cross plot	0.89	11.0	16.3	-	-	-
	Brocher (2005) equation	0.89	11.9	19.2	-	-	-
9	Fuzzy logic	0.44	36.2	38.54	0.45	36.9	39.4
	Multiple linear regression	0.58	30.7	32.68	0.58	32.7	34.8
	Neural Network	0.43	44.2	46.38	0.55	26.3	28.8
	Simple cross plot	0.60	31.0	33.00	-	-	-
	Brocher (2005) equation	0.60	12.3	15.29	-	-	-
10	Fuzzy logic	-	-	-	0.88	16.6	17.7
	Multiple linear regression	-	-	-	0.89	15.4	16.3
	Neural Network	-	-	-	0.85	4.1	5.4
	Simple cross plot	0.92	15.4	16.4	-	-	-
	Brocher (2005) equation	0.91	10.5	11.5	-	-	-

The measured basic wireline data were used as input data to predict ΔTs by using intelligent tools. These tools predicted ΔTs with a good of fit (about 90%). In addition, simple cross-plots of measured versus predicted ΔTs in the wells show that ΔTs is overestimated at dolomite lithofacies due to increasing neutron porosity. Both the simple plots and MLR models show estimated values of ΔTs lower than measured values in the dolomitic limestone and limestone lithofacies. The Brocher, (2005) equation results fit well with the measured ΔTs at dolomite and dolomitic limestone lithofacies, but the predicted ΔTs were shorter than the measured time due to the reduced porosity and the changes to the limestone lithofacies. For the anhydrite lithofacies, the intelligent tools and the Brocher equation yielded predictions of ΔTs equivalent to the measured values, but the simple plot equation provided less accurate predictions. According to that, the simple cross-plot and the Brocher equation could be used for the dolomite and dolomitic limestone lithofacies in the Facha member, particularly if no intelligent tools are available. MLR yielded results closer to the measured shear travel time than the NN results in dolomite lithofacies, but NN is more suitable for dolomitic limestone. Generally, the second PCA input data set gave better results than the first PCA input data set for the ΔTs estimated by the intelligent tools.

ACKNOWLEDGMENTS

References

Abdunaser, K. & McCaffrey, K. (2014). Rift architecture and evolution: The Sirt Basin, Libya: The influence of basement fabrics and oblique tectonics. *Journal of African Earth Sciences*, (**100**):203-226.

Abugares, Y.I. (1996). Sedimentology and hydrocarbon potential of the Gir Formation. Sirt Basin. Libya. First Symposium on the Sedimentary Basins of Libya, Geology of the Sirt Basin, vol. 2. (Eds. M. J. Salem, A. S. El Hawat, A.M. Sbeta). Amsterdam, Netherlands.

Akhundi, H., Ghafoori, M. & Lashkaripour, G.R. (2014). Prediction of shear wave velocity using artificial neural network technique, multiple regression and petrophysical data: A case study in Asmari reservoir (SW Iran). *Open Journal of Geology*, (**4**):303-313.

Ahlbrandt, T.S. (2001). The Sirte basin province of Libya: Sirte-Zelten total petroleum system: US Department of the Interior, US Geological Survey. 29p.

Ambrose, G. (2000). The geology and hydrocarbon habitat of the Sarir Sandstone, SE Sirt Basin, Libya. *Journal of Petroleum Geology*, 23(**2**):165-192.

Amiri, M.A., Conoscenti, C., & Mesgari, M.S. (2018). Improving the accuracy of rainfall prediction using a regionalization approach and neural networks. *Kuwait Journal of Science,* **45**(4):66-75.

Banerjee, S. (1980). Stratigraphic lexicon of Libya. Department of geological researches & mining. Bulletin (**13**).

Barr, F. & Weeger, A. (1972). Stratigraphic nomenclature of the Sirte Basin, Libya: Petroleum Exploration Society Libya, Tripoli. 179p.

Bateman, M.R. (2012). Openhole Log Analysis and Formation Evaluation. Society of Petroleum Engineers, United States of America. 653p.

Brocher, T.M. (2005). Empirical relations between elastic wave speeds and density in the Earth's crust. *Bulletin of the seismological Society of America*, 95(**6**), 2081-2092.

Cuddy, S. (1997). The application of the mathematics of fuzzy logic to petrophysics. Paper presented at the SPWLA 38th annual logging symposium.

Ehsan, M., Gu, H., Akhtar, M.M., Abbasi, S.S. & Ehsan, U. (2018). A geological study of reservoir formations and exploratory well depths statistical analysis in Sindh Province, Southern Lower Indus Basin, Pakistan. *Kuwait Journal of Science,* **45**(2):84-93.

Elag, M. O. (1996). Sedimentological study of the Facha Member in the southwest Sirt Basin, Libya. Paper presented at The First Symposium on the Sedimentary Basins of Libya, Geology of the Sirt Basin. Amsterdam, Netherlands.

Gras, R. (1996). Structural style of the southern margin of the Messlah High. The geology of the Sirt Basin. Amsterdam, Elsevier, (**3**):201-210.

Gras, R. & Thusu, B. (1998). Trap architecture of the Early Cretaceous Sarir sandstone in the eastern Sirt Basin, Libya. Geological Society, London, Special Publications, 132(**1**):317-334.

Greenberg, M.L. & Castagna, J.P. (1992). Shear-Wave Velocity Estimation in Porous Rocks: Theoretical Formulation, Preliminary Verification and Applications. Geophysical Prospecting, (**40**):195-209.

Guiraud, R. (1998). Mesozoic rifting and basin inversion along the northern African Tethyan margin, an overview. Geological Society, London, Special Publications, 132(**1**):217-229. Guan, Z., Sheng, Y., Luo, M., Xu, Y., Zhang, B. & Wang, Q. (2018). A new quantitative evaluation method for drilling risk based on uncertainty analysis. *Kuwait Journal of Science,* **45**(3):105-113.

Hallett, D. & Clark-Lowes, D. (2017). Petroleum geology of Libya. Elsevier, Netherlands. 393p.

Hallett, D. & El Ghoul, A. (1996). Oil and gas potential of the deep trough areas in the Sirt Basin, Libya. In Salem, M.J., El-Hawat, A.S., and Sbeta, A.M., eds., The geology of Sirt Basin: Amsterdam, Netherlands.

Harding, T. (1984). Graben hydrocarbon occurrences and structural style. AAPG Bulletin, 68(**3**):333-362.

Khamehchi, E., Kivi, I.R. & Akbari M. (2014). A novel approach to sand production prediction using artificial intelligence. *Journal of Petroleum Science and Engineering,* (**123**): 147-154.

Lashhab, M.I. & West, I.M. (1996). Dolomitization of the Jir and Rawaghah Formations in Jabal al Jir and the western Sirt Basin**.** First Symposium on the Sedimentary Basins of Libya. Geology of the Sirt Basin, vol. 2. (Eds. M.J. Salem. A.S. El-Hawat and A.M. Sbeta). Elsevier, Amsterdam, Netherlands.

Liu, H. (2017). Principles and Applications of Well Logging. In: Sonic Logs, Pp. 59-114. **Springer, China.**

Maleki, S., Moradzadeh, A., Riabi, R.G., Gholami, R. & Sadeghzadeh, F. (2014). Prediction of shear wave velocity using empirical correlations and artificial intelligence methods. *NRIAG Journal of Astronomy and Geophysics*, (**3**):70-81.

Mijalkovic, N. (1977). Geological Map of Libya, Al Qaddahiyah (NH33-3). Explanatory Booklet. Industrial Research Centre, SPL AJ. Tripoli.

Miraj, A. F. M., Ali, A., Javaid, H., Rathore, P.S., Ahsan, N., Saleem., R., Afgan, S. & Malik, B.M. (2021). An integrated approach to evaluate the hydrocarbon potential of Jurassic Samana Suk Formation in Middle Indus Basin, Pakistan. *Kuwait Journal of Science*, 48(**4**):1-11.

Olasunkanmi, N., Sunmonu, L.A. & Adabanija, M.A. (2020). Geophysical investigation for mineral prospect in Igbeti-Moro area, southwestern Nigeria. *Kuwait Journal of Science,* **47**(3):2-14.

Singh, S., Kanli, A.I. (2015). Estimating shear wave velocities in oil fields: a neural network approach. *Geosciences Journal*, DOI 10.1007/s12303-015-0036-z.

Tao, L.Z., Ming, L.Q. & Hong, Z. (2020). Integrated physical detection technology in complicated surface subsidence area of mining area. *Kuwait Journal of Science,* **47**(1):86-96.Tawadros, E. (2001). Geology of Egypt and Libya. Balkema-Rotterdam**,** Netherlands. 468p.